Geometric control of sliding friction

Liefferink, R.W.; Weber, B.; Coulais, C.; Bonn, D.

DOI
10.1016/j.eml.2021.101475
Publication date
2021
Document Version
Final published version
Published in
Extreme Mechanics Letters

Extreme Mechanics Letters 49 (2021) 101475

Contents lists available at ScienceDirect

Extreme Mechanics Letters

journal homepage: www.elsevier.com/locate/eml

Geometric control of sliding friction

Rinse W. Liefferink [a], Bart Weber [a,b,*], Corentin Coulais [a], Daniel Bonn [a]

[a] Institute of Physics, University of Amsterdam, Science Park 904, 1098 XH Amsterdam, The Netherlands
[b] Advanced Research Center for Nanolithography, Science Park 110, 1098 XG Amsterdam, The Netherlands

ARTICLE INFO

Article history:
Received 21 June 2021
Received in revised form 11 August 2021
Accepted 25 August 2021
Available online 4 September 2021

Keywords:
Friction
Topography
Metamaterials

ABSTRACT

Controlling and predicting friction is a significant scientific and technological issue. It is our everyday experience that two smooth surfaces slide more easily over each other than two rough ones, due to interlocking of the rough surfaces. However, the interpretation of such friction forces is difficult since other contributions arise from e.g. adhesion forces, that are harder to control. Here, we demonstrate that designer macroscopic roughness can be used to control, dynamically tune and quantitatively predict friction. We show that the roughness allows to tune the friction coefficient by more than an order of magnitude, which can be explained completely by a simple Coulombic friction model. A kirigami metamaterial surface with externally tunable roughness allows us to show that this understanding of geometrical friction can be used to control on-the-fly the friction in a single system by dynamically controlling its roughness.

1. Introduction

The major goal of tribology is to reduce friction and wear to increase energy efficiency [1]. For the vast majority of the surfaces encountered in nature and used in industry, the source of dry friction lies in the imperfections of the surfaces [2–4]. When rough surfaces slide over each other, the roughnesses will interlock, deform and consequently oppose the motion and generate friction [5–9]. At the same time, very smooth surfaces do not solve the problem of friction reduction either: the decrease of roughness to atomically flat level leads to a much higher friction due to an increase of the adhesion forces (van der Waals interactions, capillary forces, etc.) [10,11]. The competing effects of friction generated by roughness slopes that (almost) interlock and adhesion are notoriously difficult to disentangle, since the surface roughness typically spans all length scales from atomic to macroscopic [12–14].

Here we study the effect of interface geometry separately by macroscopic patterning, allowing to control and predict the friction that results from the interface geometry and separate it from the adhesion contributions. Tuning sliding friction by surface topography is a well developed area of research at the nanoscale [12,15–19] and at the macroscale [20–22]. Yet, a clear understanding of the role of interlocking and interface geometry vs. adhesion and hence quantitative predictions are still lacking. In many situations of practical importance, one would like to be able to control the friction of two given surfaces. We explore the ability to modify the friction force with designer surface roughness and show that the friction force can be tuned by more than an order of magnitude. We further explore the scalability and limits of such strategy as the roughness is scaled down towards the micrometer scales. Finally, we show here that by controlling the interface geometry, we can dynamically tune friction externally, without changing the slider. We achieve this by using kirigami metamaterial surfaces. Our work provides vistas for the use of geometry and metamaterials for the control of friction.

2. Method

2.1. Experimental protocol

We start by performing sliding experiments with surfaces with triangular teeth to evaluate the influence of macroscopic periodic roughness on the friction force. The macroscopic periodic roughness is fabricated on the surfaces of plastic, aluminium, stainless steel and Mylar objects (see Table S1); they are triangles with an interior angle θ and a fixed height h of 3 mm as schematically illustrated in Fig. 2. On the Mylar surfaces we created tunable kirigami patterns that will be further introduced and discussed later in the text. The top surface is pulled over a bottom surface where, for simplicity, the top surface pattern consists of a single triangular tooth. The sliding experiments are performed with a stepper motor coupled to a load cell that horizontally pulls the top surface at an imposed constant sliding speed of 1 mm/s over the bottom surface. The pulling force F_T is monitored as a function of the sliding distance d while the gravitational force

* Corresponding author at: Institute of Physics, University of Amsterdam, Science Park 904, 1098 XH Amsterdam, The Netherlands.
E-mail address: b.weber@arcnl.nl (B. Weber).

https://doi.org/10.1016/j.eml.2021.101475

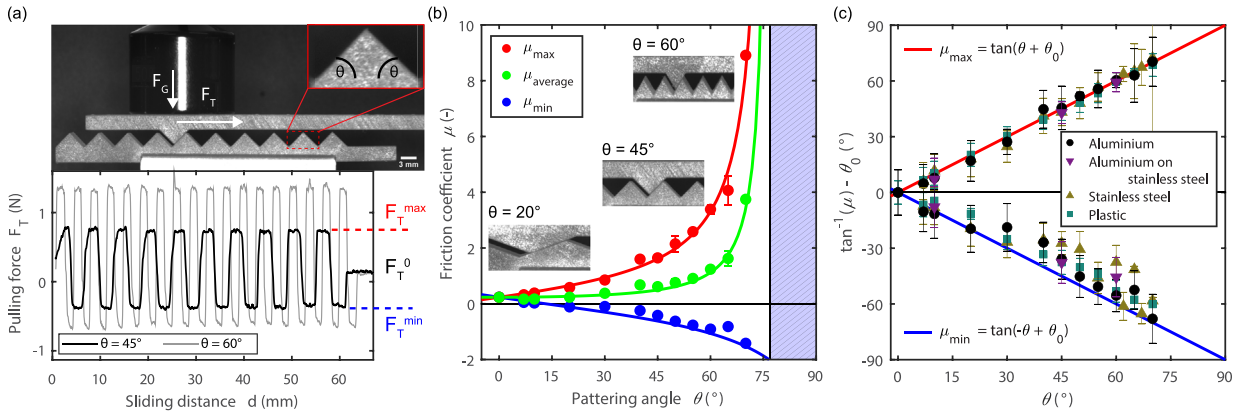

Fig. 1. Sliding experiments with triangular patterned surfaces. (a) Experimental setup visualized from the side of the sliding experiment and the monitored pulling force F_T as a function of distance d. As macroscopic roughness, a triangular pattern is fabricated with a fixed height of 3 mm and controlled angle θ. The observed square wave of the pulling force is shown for $\theta = 45°$ and $\theta = 60°$ in, respectively, black and grey. (b) Friction coefficient μ as a function of the angle θ for the maximum (red), average (green) and minimum (blue) friction, either measured (circles) or calculated (continuous lines) with Eqs. (2) to (4). (c) The maximum and minimum friction coefficient, normalized with the system-specific angle $\theta_0 = \tan^{-1}(\mu_0)$ where μ_0 is the microscopic friction coefficient, for increasing angle θ for aluminium, aluminium on stainless steel, stainless steel, and plastic sliders. The red (top) and blue (bottom) continuous lines represent the calculated maximum and minimum friction coefficient.

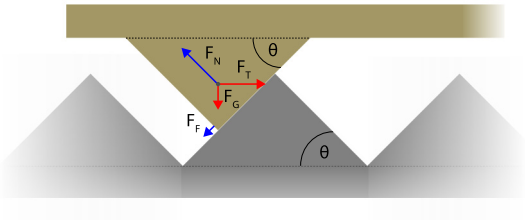

Fig. 2. Schematic illustration, including a force balance, for sliding two triangular patterned surfaces with patterning angle θ over each other. F_G is the gravitational force, F_N the normal force, F_F the friction force and F_T the horizontal pulling force.

F_G is controlled by placing dead weights on the slider; see Table S2. The microscopic surface roughness is measured using laser-scanning profilometry (Keyence VK-X1000), which allows us to estimate the root-mean-square surface height variation S_q, see Table S1 in the Supp. Mat.

2.2. Macroscopic roughness

The pulling force F_T as a function of the sliding distance d is monitored which results in a square-wave type response [Fig. 1(a) bottom]. When the slider climbs uphill over the bottom surface, a high and constant tangential force F_T^{max} is measured. Subsequently, when the top of the triangular pattern is reached, the force drops and a constant (negative) force F_T^{min} is measured as the slider slides downhill until it hits the next triangular tooth. The plateau values F_T^{max} and F_T^{min} both increase when the patterning angle θ increases. Therefore, the interface geometry leads to significant variations of the friction force and an average friction force F_T^{mean}, which is larger than that of the flat surface $F_T^0 = \mu_0 F_G$.

3. Results and discussion

3.1. Tuning friction

The roughness can be purposely changed to tune the magnitude of the friction force variations and its average. In Fig. 1(b) the influence of the angle θ is observed for maximum (red), minimum (blue) and average (green) macroscopic friction coefficient μ which is defined as the ratio of the measured tangential to the normal (gravitational) force. We find that the average friction coefficient increases by more than an order of magnitude when the patterning angle θ is varied from 20° to 60°. The influence of the angle θ on the friction coefficient can be understood by considering a simple Coulombic model. The maximum macroscopic friction coefficient, defined as the ratio of tangential to gravitational force $\mu_{max} := F_T^{max}/F_G$, can be written as

$$\mu_{max} = \frac{F_N \sin(\theta) + F_F \cos(\theta)}{F_N \cos(\theta) - F_F \sin(\theta)}, \tag{1}$$

where F_N and F_F are the normal and tangential forces experienced by the slider when sliding uphill against a triangular tooth; see Fig. 2.

The tangential force is set by the microscopic friction coefficient μ_0 as $F_F = \mu_0 F_N$. The microscopic friction coefficient is measured during flat-on-flat sliding, i.e., $\theta = 0°$, with the same materials under the same conditions and is found to be 0.23 ± 0.02 for the aluminium sliders; see Table S2. Eq. (1) can be rewritten by defining the microscopic angle θ_0 that accounts for the microscopic friction as:

$$\mu_{max} = \tan(\theta + \theta_0). \tag{2}$$

Similar to the maximum friction coefficient, the minimum and average friction coefficient can be derived likewise:

$$\mu_{min} = \tan(-\theta + \theta_0) \tag{3}$$

$$\mu_{average} = \frac{\tan(\theta + \theta_0) + \tan(-\theta + \theta_0)}{2}. \tag{4}$$

In Fig. 1(b) the model is shown as the continuous lines and captures the frictional behaviour of triangular patterned surfaces. The measured microscopic friction coefficient $\mu_0 = tan(\theta_0)$ for the aluminium sliders was used to calculate the microscopic angle $\theta_0 = 13°$. The blue (grey) dashed area in Fig. 1(b) represents the tilt angles for which the interface is interlocked and can only be brought into motion after failure of the materials through for instance fracture or adhesive wear [23,24].

The large changes of frictional force and the interlocking as roughness is increased is applicable independently of the material of choice. Aluminium, stainless steel and plastic all exhibit this generic behaviour; using different θ_0 for the different materials, a master curve can be created [see Fig. 1(c)], where the continuous lines follow from the simple geometrical model. The deviation

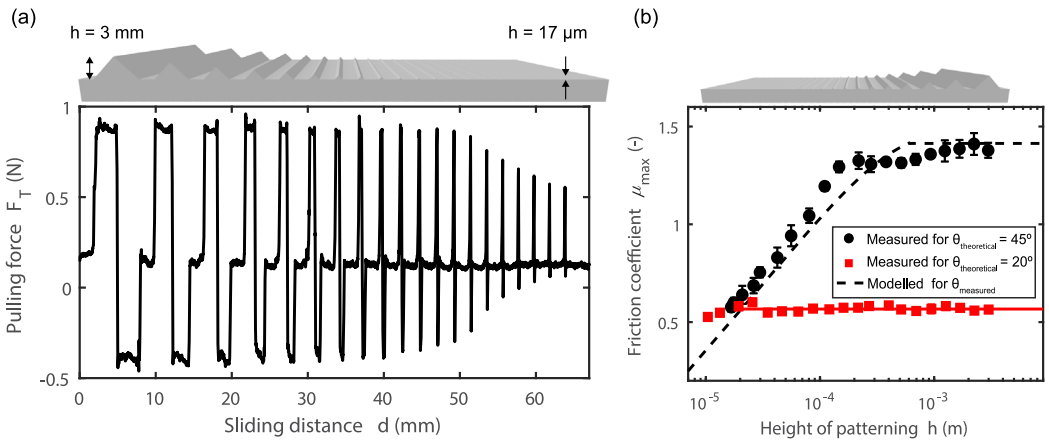

Fig. 3. (a) Pulling force F_T as a function of the sliding distance d for a triangular patterned surface fabricated in aluminium with a stepwise decreasing height h. Due to imperfections in the making process, the angle also becomes smaller when the triangles become very small. The sliding speed is set at $v = 0.05$ mm/s for an imposed gravitational load of $F_G = 0.72$ N. (b) Maximum friction coefficient μ as a function of the height h of the triangular patterned surface. The measured maximum friction coefficient is presented for surfaces with constant patterning angle $\theta_{theoretical}$ and varying patterning height. As a result of the limited resolution of the fabrication technique, the angle θ decreases significantly for decreasing patterning height. The black dashed line represents the calculated maximum friction coefficient [Eq. (2)] based on the measured angle $\theta_{measured}$ and the microscopic friction coefficient μ_0 for the specific patterning height; see S3 for more details.

between the measurements and the calculation for μ_{min} is likely a result of a small tilt of the slider when it slides down along the triangular pattern. In addition, we have extended the geometrical friction model to interfaces at which the roughness is no longer commensurable, i.e. the angles and heights at the top and bottom surfaces are different, see S2. Taking a bottom surface with systematically varying height and angle of the triangles, we find that the sliding friction is controlled by the lowest angle θ of the two surfaces. In conclusion, designed roughness is a powerful strategy to tune friction by controlling the local surface slope of the sliding surfaces.

3.2. Scalability of geometrical control of friction

The control over frictional forces via interface geometry and its quantitative understanding is promising, and the question is to what microscopic length scale we can push this. To address this question, we systematically decrease the scale of the roughness. To this end, we pattern an aluminium surface with decreasing patterning height, from 3 mm to 17 µm; see Fig. 3(a). We pull an aluminium top surface with a single tooth, height of 3 mm and angle θ_T of 45°, over the patterned surface and measure the pulling force. To resolve the monitored friction force even for the smallest sawteeth, the sliding speed at which the smallest peaks are measured is decreased down to 0.05 mm/s. As previously, we observe plateaus in the measured pulling force for the largest sawteeth on the substrate. As the teeth become smaller, the friction plateaus cover a smaller distance and start to look more like friction peaks. However, the friction peak force corresponding to the smallest teeth with heights down to 17 µm no longer matches the friction plateau heights measured for larger teeth with the same angle. We show the maximum friction coefficient as a function of the patterning height h, shown as black circles in Fig. 3(b). As expected, the sliding friction for a triangular pattern with a height of $\approx$ 0.2–3 mm is in agreement with the model, represented with the horizontal part of the dashed line. For smaller heights, there is a significant deviation. Such a deviation is not visible if we pattern the surface with a smaller angle of $\theta_T = 20°$.

The decrease of the sliding friction for the $\theta_T = 45°$ surface when the height of the triangular tooth is smaller than 200 µm [Fig. 3(b)] can in fact be explained with the limited resolution of the fabrication technique. Both the actual patterning angle θ and the surface roughness S_q change as the teeth become smaller. When an angle $\theta = 45°$ is aimed for, the actual angle is smaller when the teeth are small (Fig. S2). In addition to a decrease of the angle θ for smaller patterns, an increase in surface roughness is observed (Fig. S3), which results in an increase of the microscopic friction coefficient μ_0 (see S3 for a detailed discussion). When using the actual values of the macroscopic and microscopic coefficients in our geometrical friction model, the observed variation of the friction coefficient μ_{max} [dashed lines in Fig. 3(b)] is well reproduced. The decrease of the measured friction coefficient for smaller patterns is therefore the result of a decrease of the actual angle θ which is partly compensated by an increase of the surface roughness and is the result of limited fabrication resolution. This also explains why the data for $\theta_T = 20°$ agree with the model; the manufactured angle is much closer to the target value. The data are therefore in good agreement with the expected maximum friction coefficient μ_{max} [Eq. (2)] that is represented in Fig. 3(b) as the red (continuous) line. Therefore, with a smaller designed angle θ the friction can be tuned. In conclusion, designer roughness is an efficient strategy to artificially increase friction, but is ultimately limited by the manufacturing techniques employed. A fine characterization of the surface topography at multiple scales does however allow for a quantitative prediction of the friction force with our model, down to length scales of several tens of micrometers. The fact that we still need a microscopic friction coefficient to describe the data implies that Coulombic or adhesive friction on smaller scales still contributes significantly to the measured friction force.

3.3. On-the-fly control of geometrical friction

As mentioned in the introduction and methods section, we further explored the possibility of dynamic friction control through kirigami patterning of the sliding surfaces. In kirigami, the surface roughness can be controlled externally by stretching the material [25–27]. Rafsanjani et al. made use of this technique to tune on-demand the texturing of a kirigami metamaterial sheet [22]. The authors designed a bioinspired robotic snake that, due to repeated stretching and releasing of the kirigami skin that forms triangular scales when stretched, can crawl forward, similar to a real snake [28–31]. The formation of on-demand texturing, based on kirigami scales that point out-of-plane, is

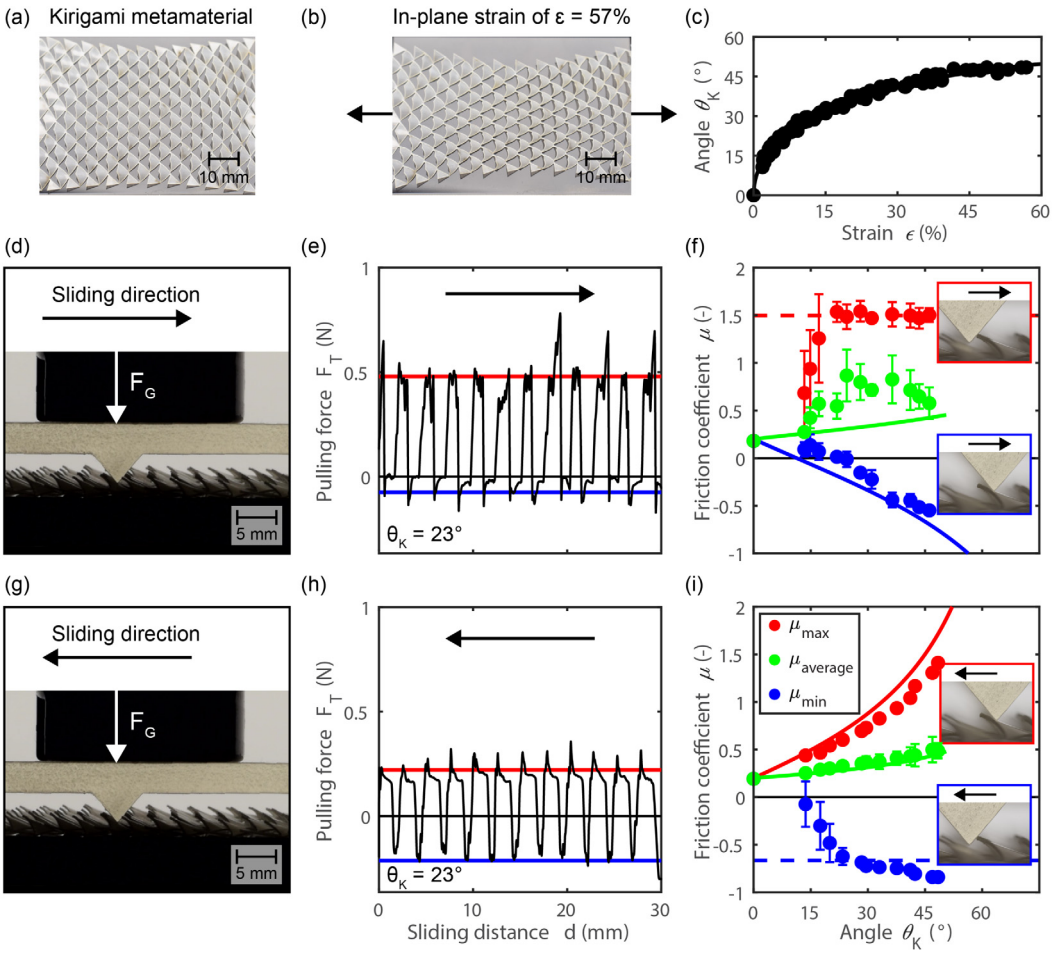

Fig. 4. Sliding experiments on a kirigami metamaterial. (a) A kirigami patterning is laser-cut in a Mylar sheet. (b) A macroscopic out-of-plane surface roughness, i.e., scales pointing outwards, can be actuated for increasing in-plane uniaxial strain ϵ. (c) kirigami angle θ_K for increasing strain ϵ. The black continuous line is a fit, see S5 for more details. (d) Side-view of the sliding experiment when sliding against the formed kirigami scales. The slider has a single triangular tooth pattern with an angle of $\theta_T = 45°$. (e) Pulling force F_T as a function of the sliding distance d when the slider is pulled against the kirigami scales pointing upward with an angle of $\theta_K = 23°$. In continuous red (top) and blue (bottom) lines, the calculated friction coefficient for, respectively, the maximum [Eq. (2)] and minimum [Eq. (2)]. (f) Friction coefficient μ as a function of the measured kirigami angle θ_K for sliding against the scales. In continuous lines the calculated friction coefficients are shown [Eqs. (2), (3), and (S4)]. (g–i) The sliding experiment when performed along the kirigami scales.

very similar to the triangular tooth patterns. The kirigami metamaterial surface then allows to tune the friction by externally controlling its roughness.

To get control over the roughness, we laser cut a mylar sheet with a triangular pattern (see S4 for more experimental details) and perform sliding experiments while controlling the in-plane uniaxial strain ϵ on the metamaterial surface: the larger the strain, the more the scales will stick out with a large angle. In Fig. 4(a) and (b) we show the kirigami metamaterial for zero and large strain. The scales point upwards with an angle θ_K that can be quantified visually from the side; see Fig. 4(c). We perform sliding experiments with a single triangular tooth ($\theta_T = 45°$) patterned surface pulled horizontally along the kirigami scales as shown in, respectively, Fig. 4(d) and (g).

The measured pulling forces again roughly have a square wave shape, similarly as was found for the triangular tooth patterned surfaces [Fig. 4(e) and (h)]. The square wave is distorted by periodic peaks in the pulling force, which correspond to the moment at which the slider snaps from the top of the kirigami scales and after which the force reaches a plateau. These plateaus allow once more to define the maximum, minimum, and average friction coefficients and to plot it as a function of θ_K [Fig. 4(f) and (i)] for the same kirigami stretched to various strains, hence with various roughness angles θ_K. To quantitatively capture these results we apply the exact same geometrical friction model as before for the triangular teeth with the important distinction that the slope between friction force and sliding direction is redefined according to the geometry of the kirigami teeth (S5). Importantly, our model again accurately predicts the tunable friction

Again, the smallest angle θ, that is either the kirigami scale angle θ_K or the angle of the top surface θ_T, sets the friction coefficient. Due to the anisotropic nature of the scales, we find that the measured maximum and minimum friction coefficient are also very anisotropic: they depend on the sliding direction and show strongly asymmetric friction, as also expected from our model.

In addition, the measured average friction coefficient [shown as the green (colour online) circles in Fig. 4(f)] is very high and seems to be rather θ_K-independent when sliding against the pattern. In contrast, it increases smoothly with θ_K when sliding with the pattern, shown in Fig. 4(i). The high and rather constant value of the friction coefficient when sliding against the pattern is likely due to the compliance of the kirigami scales; as the slider builds up the friction force, the scales are bend upwards leading to a larger angle and a larger friction force than calculated. A similar but opposite effect can be noted in Fig. 4(i) where the measured maximum friction is slightly lower than the calculated friction. Nonetheless, the asymmetry of the kirigami metamaterial decreases with increasing strain and can be geometrically

calculated, as discussed in S5. The green (colour online) lines in Fig. 4(f) and (i) are the weighted average friction coefficient based on the asymmetric path lengths [respectively Eqs. (S4) and (S5)]. Thus, also the kirigami metamaterial surfaces agree with the simple picture of Coulombic geometrical friction presented here.

4. Discussion

The influence of macroscopic geometrical patterns on friction can be applied to various tribological systems; earthquake dynamics [4,5] and anisotropic friction by surface patterns [32,33] have been modelled based on their macroscopic surface geometry. A similar model has been introduced to describe the microscopic friction coefficient based on the surface height variations of surfaces [34,35]. However, modelling the influence of the surface roughness with this geometrical model was not satisfactory; the real contact area that is formed and the shear stress prior to sliding on the asperity-level is rather more complex [36]. In the model presented here, we separate the rather complex (adhesive) friction coefficient μ_0 from the geometrical part for macroscopic surface roughness.

With the artificial macroscopic surface roughness the sliding friction can be tuned by more than an order of magnitude, which can in addition be explained using a simple geometrical model that takes into account the geometry-dependent Coulombic friction between the two surfaces. The slope, quantified with the angle, of the surface patterning and the commensurability of patterned surfaces enables direct control on the sliding friction. In addition, a kirigami metamaterial surface allows to apply this understanding of geometrical friction to enable external and on-demand control of the friction force. The understanding of how friction can be tuned with macroscopic surface patterns can be valuable for applications in locomotion, such as modulating the friction of a shoe sole with designed surface patterns [27], or for applications in finger–surface contact in which the interplay between grip and surface texturing can be exploited [20].

5. Conclusion

In summary, we have presented sliding experiments of sliders with macroscopic surface patterning and shown the influence of the patterning slope of the surfaces. A simple geometrical model describes the measured sliding friction based on the macroscopic geometry together with the microscopic friction coefficient μ_0.

Declaration of competing interest

The authors declare the following financial interests/personal relationships which may be considered as potential competing interests: Rinse Liefferink reports financial support was provided by Shell.

Acknowledgements

R.W.L. thanks Shell for financial support (PT 67354). B.W. acknowledges funding from the Netherlands Organization for Scientific Research (NWO) VENI grant no. VI.Veni.192.177. The authors thank Shahin Rouhani for very helpful discussions and Daan Haver and Menno Demmenie for performing preliminary experiments.

Appendix A. Supplementary data

Supplementary material related to this article can be found online at https://doi.org/10.1016/j.eml.2021.101475.

References

[1] K. Holmberg, A. Erdemir, Influence of tribology on global energy consumption, costs and emissions, Friction 5 (3) (2017) 263–284.
[2] I. Sherrington, E.H. Smith, The significance of surface topography in engineering, Precis. Eng. 8 (2) (1986) 79–87.
[3] T.R. Thomas, T.R. Thomas, Rough Surfaces, Vol. 278, World Scientific, 1999.
[4] E.E. Brodsky, J.J. Mori, L. Anderson, F.M. Chester, M. Conin, E.M. Dunham, N. Eguchi, P.M. Fulton, R. Hino, T. Hirose, M.J. Ikari, T. Ishikawa, T. Jeppson, Y. Kano, J. Kirkpatrick, S. Kodaira, W. Lin, Y. Nakamura, H.S. Rabinowitz, C. Regalla, F. Remitti, C. Rowe, D.M. Saffer, S. Saito, J. Sample, Y. Sanada, H.M. Savage, T. Sun, S. Toczko, K. Ujiie, M. Wolfson-Schwehr, T. Yang, The state of stress on the fault before, during, and after a major earthquake, Annu. Rev. Earth Planet. Sci. 48 (1) (2020) 49–74.
[5] T. Pöschel, H.J. Herrmann, A simple geometrical model for solid friction, Physica A 198 (3–4) (1993) 441–448.
[6] R. Grönqvist, Mechanisms of friction and assessment of slip resistance of new and used footwear soles on contaminated floors, Ergonomics 38 (2) (1995) 224–241.
[7] P.L. Menezes, S.V. Kailas, M.R. Lovell, Role of surface texture, roughness, and hardness on friction during unidirectional sliding, Tribol. Lett. 41 (1) (2011) 1–15.
[8] G.A. Pilkington, E. Thormann, P.M. Claesson, G.M. Fuge, O.J. Fox, M.N. Ashfold, H. Leese, D. Mattia, W.H. Briscoe, Amontonian frictional behaviour of nanostructured surfaces, Phys. Chem. Chem. Phys. 13 (20) (2011) 9318–9326.
[9] J. Jiang, R.D. Arnell, The effect of substrate surface roughness on the wear of DLC coatings, Wear 239 (1) (2000) 1–9.
[10] H. Spikes, Stress-augmented thermal activation: Tribology feels the force, Friction 6 (1) (2018) 1–31.
[11] S.M. Rubinstein, G. Cohen, J. Fineberg, Visualizing stick–slip: experimental observations of processes governing the nucleation of frictional sliding, J. Phys. D: Appl. Phys. 42 (21) (2009) 214016.
[12] M. Dienwiebel, G.S. Verhoeven, N. Pradeep, J.W. Frenken, J.A. Heimberg, H.W. Zandbergen, Superlubricity of graphite, Phys. Rev. Lett. 92 (12) (2004) 126101.
[13] H.A. Spikes, Mixed lubrication—an overview, Lubr. Sci. 9 (3) (1997) 221–253.
[14] D. Petrova, B. Weber, C. Allain, P. Audebert, C.H. Venner, A.M. Brouwer, D. Bonn, Fluorescence microscopy visualization of the roughness-induced transition between lubrication regimes, Sci. Adv. 5 (12) (2019) eaaw4761.
[15] J.M. Martin, C. Donnet, T. Le Mogne, T. Epicier, Superlubricity of molybdenum disulphide, Phys. Rev. B 48 (14) (1993) 10583.
[16] A. Erdemir, O. Eryilmaz, Achieving superlubricity in DLC films by controlling bulk, surface, and tribochemistry, Friction 2 (2) (2014) 140–155.
[17] S. Zhang, Y. Hou, S. Li, L. Liu, Z. Zhang, X.-Q. Feng, Q. Li, Tuning friction to a superlubric state via in-plane straining, Proc. Natl. Acad. Sci. 116 (49) (2019) 24452–24456.
[18] M.R. Vazirisereshk, K. Hasz, R.W. Carpick, A. Martini, Friction anisotropy of MoS2: Effect of tip–sample contact quality, J. Phys. Chem. Lett. 11 (16) (2020) 6900–6906.
[19] M.Z. Baykara, M.R. Vazirisereshk, A. Martini, Emerging superlubricity: A review of the state of the art and perspectives on future research, Appl. Phys. Rev. 5 (4) (2018) 041102.
[20] S.E. Tomlinson, M. Carré, R. Lewis, S.E. Franklin, Human finger contact with small, triangular ridged surfaces, Wear 271 (9–10) (2011) 2346–2353.
[21] L.-W. Liu, Y.H. Lee, C.J. Lin, K.W. Li, C.Y. Chen, Shoe sole tread designs and outcomes of slipping and falling on slippery floor surfaces, PLoS One 8 (7) (2013) e68989.
[22] A. Rafsanjani, Y. Zhang, B. Liu, S.M. Rubinstein, K. Bertoldi, Kirigami skins make a simple soft actuator crawl, Science Robotics 3 (15) (2018).
[23] R. Aghababaei, D. Warner, J.F. Molinari, Critical length scale controls adhesive wear mechanisms, Nature Commun. 7 (1) (2016) 11816.
[24] M. Malekan, M.K. Budzik, H.M. Jensen, R. Aghababaei, Fracture analyses of surface asperities during sliding contact, Tribol. Int. 159 (2021) 106939, http://dx.doi.org/10.1016/j.triboint.2021.106939, URL https://www.sciencedirect.com/science/article/pii/S0301679X21000876.
[25] A. Rafsanjani, K. Bertoldi, Buckling-induced kirigami, Phys. Rev. Lett. 118 (8) (2017) 084301.
[26] Y. Yang, M.A. Dias, D.P. Holmes, Multistable kirigami for tunable architected materials, Phys. Rev. Mater. 2 (11) (2018) 110601.
[27] S. Babaee, S. Pajovic, A. Rafsanjani, Y. Shi, K. Bertoldi, G. Traverso, Bioinspired kirigami metasurfaces as assistive shoe grips, Nat. Biomed. Eng. 4 (8) (2020) 778–786.
[28] D.L. Hu, J. Nirody, T. Scott, M.J. Shelley, The mechanics of slithering locomotion, Proc. Natl. Acad. Sci. 106 (25) (2009) 10081–10085.
[29] H. Marvi, D.L. Hu, Friction enhancement in concertina locomotion of snakes, J. R. Soc. Interface 9 (76) (2012) 3067–3080.
[30] H.T. Tramsen, S.N. Gorb, H. Zhang, P. Manoonpong, Z. Dai, L. Heepe, Inversion of friction anisotropy in a bio-inspired asymmetrically structured surface, J. R. Soc. Interface 15 (138) (2018) 20170629.

[31] S. Ma, M. Scaraggi, C. Yan, X. Wang, S.N. Gorb, D. Dini, F. Zhou, Bioinspired 3D printed locomotion devices based on anisotropic friction, Small 15 (1) (2019) 1802931.
[32] Z. Mróz, S. Stupkiewicz, An anisotropic friction and wear model, Int. J. Solids Struct. 31 (8) (1994) 1113–1131.
[33] N. Antoni, J.-L. Ligier, P. Saffré, J. Pastor, Asymmetric friction: Modelling and experiments, Internat. J. Engrg. Sci. 45 (2–8) (2007) 587–600.
[34] J.E. Field, The Properties of Diamond, Academic Press, 1979, pp. 342–350.
[35] I.J. Ford, Roughness effect on friction for multi-asperity contact between surfaces, J. Phys. D: Appl. Phys. 26 (12) (1993) 2219.
[36] B.N.J. Persson, Theory of rubber friction and contact mechanics, J. Chem. Phys. 115 (8) (2001) 3840–3861.